



# A highly efficient nanoporous BiVO<sub>4</sub> photoelectrode with enhanced interface charge transfer Co-catalyzed by molecular catalyst

Miao Kan, Dongqi Xue, Aihua Jia, Xufang Qian, Dongting Yue, Jinping Jia, Yixin Zhao\*

School of Environmental Science and Engineering, Shanghai Jiao Tong University, 800 Dongchuan Road, Shanghai 200240, China

## ARTICLE INFO

### Keywords:

Water splitting  
Charge transfer  
BiVO<sub>4</sub>  
Molecular catalysts  
ALD

## ABSTRACT

A highly efficient nanoporous non-doped BiVO<sub>4</sub> photoelectrode with high photocurrent and low onset potential for photoelectrochemical water splitting was achieved by using molecular catalyst and amorphous TiO<sub>2</sub> stabilization layer. This BiVO<sub>4</sub> photoelectrode co-catalyzed by molecular catalyst of Ir-COOH exhibits the photoelectrochemical performance comparable to the limitation values obtained in Na<sub>2</sub>SO<sub>3</sub> sacrifice agent. Interestingly, the BiVO<sub>4</sub>/Ir-COOH exhibits more efficient interface charge transfer than BiVO<sub>4</sub>/IrO<sub>x</sub> as measured by intensity modulated photocurrent spectroscopy (IMPS) and intensity modulated photovoltage spectroscopy (IMVS) although the Ir-COOH molecular catalyst shows much lower electrochemically catalytic activities than the state-of-the-art IrO<sub>x</sub> nanoparticles for water splitting. The Ir-COOH/BiVO<sub>4</sub> was further stabilized by double amorphous TiO<sub>2</sub> layers with little impact on charge transfer. In all, it is promising to achieve high efficiency water splitting by using molecular catalysts to co-catalyze nanostructure photoelectrodes with short diffusion length and such system can be stabilized by amorphous TiO<sub>2</sub> layer.

## 1. Introduction

Photoelectrochemical (PEC) water splitting, using photocathode and photoanode to produce H<sub>2</sub> and O<sub>2</sub> respectively, is one of promising solar energy conversion approach for renewable energy [1–4]. Generally, the efficiency of PEC water splitting cell is mainly limited by the photoelectrodes' material properties including light absorption, diffusion length and stabilities [5]. Consequently, lots of research effort and attention have been investigated to explore all kinds of semiconductor materials as candidates for photoelectrodes [6]. For example, lots of n type semiconductor materials especially different metal oxides have been developed and used as photoanodes [7,8]. But, it is difficult to find an ideal photoanodes materials with all desired properties. For example, BiVO<sub>4</sub> has attracted tremendous research attention as one of promising photoanode with advantages of suitable direct band gap, high activities and low cost [9–11]. But the short diffusion length of BiVO<sub>4</sub> seriously deteriorates its water splitting efficiency, which is common for lots of novel photoelectrodes [12,13]. Different methods especially chemical doping has developed to modify its intrinsic properties to enhance BiVO<sub>4</sub> photoelectrodes' electron transfer properties [14–16].

Besides the intrinsic modification on electron structure of BiVO<sub>4</sub>, extrinsic manipulation such as nanostructure adjustment to increase surface area and morphology control to shorten charge transport

distance can improves the charge transfer efficiency of BiVO<sub>4</sub> photoanode [17,18]. Another popular strategy is to incorporate co-catalysts onto BiVO<sub>4</sub> to improve the charge separation and reduce the overpotential for water oxidations [19,20]. In order to obtain higher catalytic performance, nanostructured noble metal based co-catalysts are usually deposited onto the nanostructured BiVO<sub>4</sub> photoanodes [21–24]. The molecular catalysts with nearly 100% atomic activities have been widely developed and used in dye sensitized photocatalysis or electrochemical catalysis, but their electrochemically catalytic activities are usually lower than noble metal based nanoparticles. [25–29] However, the molecular catalysts have one unique advantages over nanoparticles: molecular catalysts can be homogeneously arched to photoelectrode's surface with designed functional linker groups, while the nanoparticles are easy to agglomerate on top surface during deposition. In this report, we use both Ir molecular catalysts of Ir-COOH and the state-of-the-art colloidal IrO<sub>x</sub> nanoparticles as oxygen evolution reaction (OER) catalysts to co-catalyze nanoporous BiVO<sub>4</sub> photoanode. Interestingly, the Ir molecular catalyst with lower electrochemically catalytic activities exhibited much better PEC catalytic activities on BiVO<sub>4</sub> photoelectrodes because of efficient charge transfer. To stabilize the nanoporous BiVO<sub>4</sub> photoelectrode co-catalyzed by Ir-COOH, the amorphous TiO<sub>2</sub> double layers have also been adopted to stabilize both BiVO<sub>4</sub> photoelectrodes' under-layer and the co-catalysts [30–33].

\* Corresponding author.

E-mail address: [Yixin.Zhao@sjtu.edu.cn](mailto:Yixin.Zhao@sjtu.edu.cn) (Y. Zhao).

## 2. Experimental

### 2.1. Preparation of BiVO<sub>4</sub> electrodes

3.32 g KI was dissolved in 45 mL DI water and adjusted to at pH ~ 1.7 using 0.1 M HNO<sub>3</sub> under stirring, 0.97 g Bi(NO<sub>3</sub>)<sub>3</sub> was added in the above solution. This orange-red solution was mixed with 20 mL of anhydrous ethanol containing 0.23 M benzoquinone (PBQ), and was well stirred or ultrasonic for a few minutes. And FTO pieces (1 × 2 cm<sup>2</sup>, 15 ohm cm) were cleaned in ethanol and water under sonication. A three-electrode system was used for electrodeposition. Here, after liner sweeping deposition from 0.3 V to -0.2 V at a scanning rate of 0.1 V/s, cathodic deposition was performed at -0.1 V vs. Ag/AgCl for 300 s to electroplate red BiOI on the working electrode at RT. 0.2 mL of a DMSO solution containing 0.2 M vanadyl-acetylacetonate was placed the BiOI electrode (1 cm × 1.5 cm) and was heated in two steps to 450 °C in a furnace (280 °C, ramping rate = 1 °C/min and 450 °C, 2 °C/min) and maintain for 2 h in air to form BiVO<sub>4</sub>. Excessive V<sub>2</sub>O<sub>5</sub> residue on the BiVO<sub>4</sub> electrodes was removed by soaking them in 1 M NaOH solution for 30 min with gentle stirring. The resulting phase pure BiVO<sub>4</sub> electrodes were rinsed with DI water and dried at RT. [18]

### 2.2. Preparation of BiVO<sub>4</sub>/TiO<sub>2</sub> electrodes

The conformal TiO<sub>2</sub> layers were deposited on taps controlled exposed nanoporous BiVO<sub>4</sub> by atomic layer deposition system (ALD f-100-4, MNT). In detail, 27 Pa as the basic vacuum situation of a heated reaction chamber with 160 °C was used with 200 ms Tetrakis (dimethylamino) titanium (TDMAT) (85 °C) and 15 ms water vapour (40 °C) with waiting time of 5 s for the ALD deposition of TiO<sub>2</sub>. And the terminal thickness is controlled by applied cycles. Each cycle would deposit ~0.625 Å thick TiO<sub>2</sub> layer in average on planar Si as confirmed by Variable Angle Spectroscopic Ellipsometer (W-VASE with AutoRetarder).

### 2.3. Synthesis of the Ir molecular catalyst and IrO<sub>x</sub> nanoparticles

The Iridium dimer [IrCl<sub>2</sub>(Cp\*)]<sub>2</sub> and 4,4'-dicarboxy-2,2'-bipyridine (H<sub>2</sub>dcabpy) were purchased from Sigma-Aldrich Co., and used as received. The solid orange-yellow chloral complex [(H<sub>2</sub>dcabpy)IrIII(Cp\*)Cl]Cl (Ir-COOH) was synthesized and purified accordingly by literature [25]. 1 mmol 4,4'-dicarboxylic acid-2,2'-bipyridine in 0.5 mL water containing 2 mmol NaOH was slowly added to a mixture of [IrIII(Cp\*)Cl<sub>2</sub>]<sub>2</sub> dimer (0.399 g, 0.5 mmol) in MeOH (15 mL) stirred for 15 min under argon. The mixture was further stirred for 3 h at 45–50 °C. The solution was cooled to room temperature and the pH was lowered to 1–2 by addition of HCl. The free ligand was filtered off and the solvent mixture was evaporated under vacuum. The solid orange-yellow chloro complex [(H<sub>2</sub>dcabpy)IrIII(Cp\*)Cl]Cl thus obtained was re-precipitated from MeOH, EtOH or acetone by addition of ether/hexane.

IrO<sub>x</sub> nanoparticle solution was prepared by alkaline hydrolysis of K<sub>2</sub>IrCl<sub>6</sub> solution: 2 mM K<sub>2</sub>IrCl<sub>6</sub> solution was dissolved in 12 mM NaOH and then heated to 90 °C followed by immediately ice bath, and the solution was then slowly turn into deep blue. The solution was then stored in refrigerator at 2 °C [22].

### 2.4. Immobilization of Ir-COOH and IrO<sub>x</sub>

1 mM Ir-COOH catalyst solution was prepared by dissolving Ir-COOH in 0.1 M aqueous NaOH solution stirred for 30 min. Then a simple soaking method was used to prepare the surface loading of BiVO<sub>4</sub> electrode. Here, the catalyst surface coverage of 5 × 10<sup>-8</sup> mol cm<sup>-2</sup> (~1.66 × 10<sup>-9</sup> mol cm<sup>-2</sup> min<sup>-1</sup>, ~50 nmol cm<sup>-2</sup> in 30 min) on sample was obtained by immersing sample in a 20 mL 0.1 mM Ir-COOH alkaline solution. The resulting Ir-COOH

loaded BiVO<sub>4</sub> were rinsed gently with DI water and dried at RT. A suitable amount of IrO<sub>x</sub> with Ir atomic concentration of ~2 × 10<sup>-8</sup> mol cm<sup>-2</sup> min<sup>-1</sup>, ~600 nmol cm<sup>-2</sup> was also deposited on BiVO<sub>4</sub> electrodes by dip soaking.

### 2.5. Physical characterization

The UV-vis spectra were recorded on an Agilent Cary 60 Scan microscope. XRD measurements were performed on a Lab XRD-6100 X-ray diffract meter. SEM and EDS mapping were performed on a Sirion 200 Field-emission Scanning Electron Microscopy. TEM images were performed with an FEI microscope.

### 2.6. Electrochemical measurements

The electrochemical activity of the IrO<sub>x</sub> and Ir-COOH catalysts were measured in 0.5 M Na<sub>2</sub>SO<sub>4</sub> electrolyte with 0.2 M pH 7 phosphate buffer solution by rotating disk electrode (RDE) using Ag/AgCl as reference and Pt wire as counter. Liner polarization curves were measured between 0.2 V and 1.2 V vs. RHE at a scan rate of 10 mV/s, and all curves were measured by Zahner Instrument with resistance correction. Electron Impedance Spectrum (EIS) were done from 500 KHz to 0.1 Hz with 0.6 V vs. RHE with slow water oxidation. For convenience, the potential of Ag/AgCl was converted into RHE by the following Equation. Intensity Modulated Photocurrent/Photovoltage Spectroscopy (IMPS/IMVS) were measured to compare the electron transport and recombination dynamics in BiVO<sub>4</sub>/TiO<sub>2</sub>/Ir-COOH/TiO<sub>2</sub> and BiVO<sub>4</sub>/TiO<sub>2</sub>/Ir-COOH/TiO<sub>2</sub> half cells. The electron transit time (τ<sub>d</sub>) and electron lifetime (τ<sub>n</sub>) in cell devices can be obtained by τ<sub>d</sub> = 1/2πf<sub>IMPS</sub>, and τ<sub>n</sub> = 1/2πf<sub>IMVS</sub>, where f<sub>IMPS</sub>/f<sub>IMVS</sub> is the frequency of the minimum imaginary component in IMPS/IMVS measurements. These measurements were performed with 430 nm LED light source from 100 K to 1 Hz.

$$E(\text{vs RHE}) = E(\text{vs Ag/AgCl}) + E_{\text{Ag/AgCl}}(\text{reference}) + 0.0591 \times \text{pH} \quad (1)$$

$$E_{\text{Ag/AgCl}}(\text{reference}) = 0.1976 \text{ V vs NHE at } 25^\circ\text{C} \quad (2)$$

## 3. Results and discussions

### 3.1. Morphology and PEC performance of undoped nanoporous BiVO<sub>4</sub> films

To exclude the other factors such as the doping variation impacting the electron transfer properties, we adopted an undoped nanoporous BiVO<sub>4</sub> (BVO) in this study. The nanoporous BiVO<sub>4</sub> photoanodes with high surface area were obtained via a two-step methods, in which the BiOI precursor films were first electrodeposited and then converted into BiVO<sub>4</sub> with intercalation of vanadium [18]. The XRD patterns (Fig. 1a) show the electrodeposited BiOI can be effectively converted to phase pure BiVO<sub>4</sub>. The electrodeposited BiOI nanoflakes are up-right as shown in Fig. 1b, which are favorable for the intercalation of vanadium precursor with enough space for volume expansion. Consequently, a nanoporous BiVO<sub>4</sub> film with ~100–200 nm sized nanocrystals is obtained, and its thickness is about 400 nm (as shown in Fig. S1). The ~400 nm thickness is within an ideal range for the undoped BiVO<sub>4</sub> photoelectrode [34]. The elemental ratio of Bi: V in this film obtained by EDS is around 1:1 as listed in Fig. S2, which is consistent with its XRD patterns. In Fig. 1c, the UV-vis spectrum of BiVO<sub>4</sub> shows a typical absorbance onset at around 520 nm and the calculated band gap of BiVO<sub>4</sub> is around 2.41 eV. To test the photo-electron conversion theoretical limitation, this nanoporous BiVO<sub>4</sub> photoelectrode was tested in the electrolyte using Na<sub>2</sub>SO<sub>3</sub> as sacrificial agent [15]. A maximum photocurrent density of 3.3 mA/cm<sup>2</sup> at 1.23 V vs RHE and ~0.2 V vs RHE onset potential are obtained in Na<sub>2</sub>SO<sub>3</sub> solution. However, the BiVO<sub>4</sub> tested for a real PEC water splitting then only a photocurrent of 1.1 mA/cm<sup>2</sup> with ~400 mV higher onset potential than BiVO<sub>4</sub>/Na<sub>2</sub>SO<sub>3</sub>

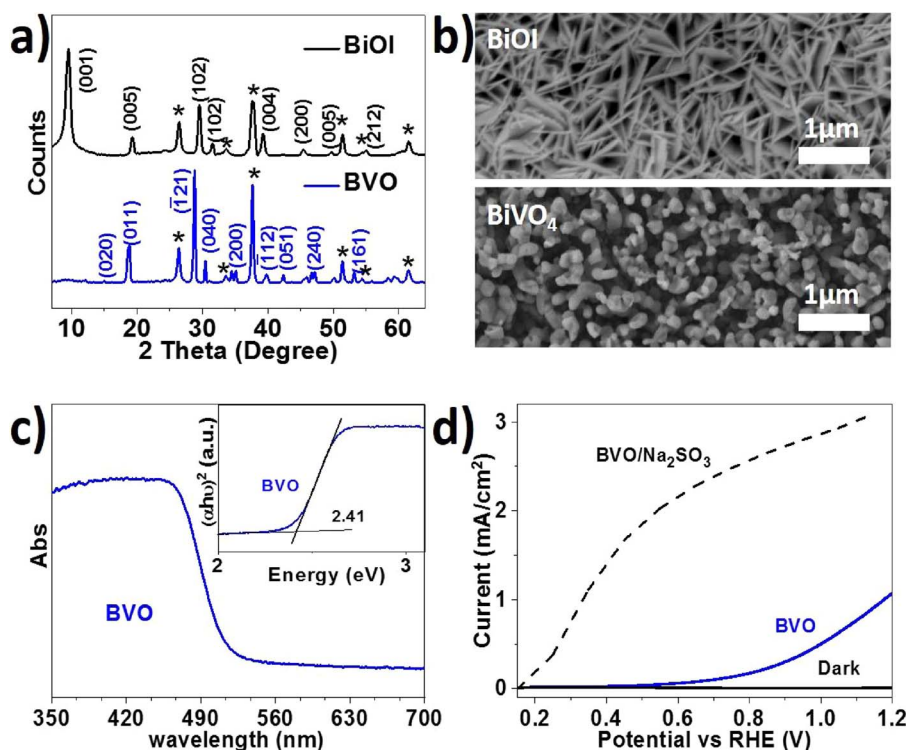


**Fig. 1.** a) XRD analysis of BiOI and BiVO<sub>4</sub> (\*, FTO); b) Top-view image of electrodeposited BiOI and prepared BiVO<sub>4</sub>; c) UV-vis spectra of pristine BiVO<sub>4</sub> with calculation of band gap in the inset; d) J-V curves of BiVO<sub>4</sub> in PBS with and without Na<sub>2</sub>SO<sub>3</sub>.

as listed in Fig. 1d. The lower photocurrent and higher onset potential is similar to previously reported undoped BiVO<sub>4</sub> photoelectrodes, which is due to the typical shortage of pristine BiVO<sub>4</sub> including quick electron-hole recombination, low charge separation and slow electron transfer.

### 3.2. Activities of Ir-COOH molecular catalysts and its effect on BiVO<sub>4</sub> electrodes

The molecular structure of the Ir-COOH is listed in Fig. 2a, which has been previously reported [25]. This figure lists the UV-vis spectra of IrO<sub>x</sub> nanoparticles and molecular catalyst of Ir-COOH, both exhibited a typical spectrum similar to previous reports. Their UV-vis spectrum (Fig. S3) can be used to characterize the catalysts loading and these values were also confirmed by ICP elemental analysis. The size of colloidal IrO<sub>x</sub> nanoparticles are 2–5 nm as confirmed in TEM image but they are easy to agglomerate when they were deposited onto photoelectrodes such as a planar Si as shown in Fig. S4. The NMR data of the Ir-COOH is consistent with previous report [27]. The rotating ring disk electrode measurements in Fig. 2b show that the IrO<sub>x</sub> nanoparticles exhibited only ~230 mV overpotential for water oxidation and is close to the state of art value for IrO<sub>x</sub> nanoparticles. While the Ir-COOH show a more than 400 mV overpotential for OER suggesting a lower activity.

Although the electro-catalytic OER activity of IrO<sub>x</sub> seems much

better than that the molecular catalyst Ir-COOH, their co-catalytic performance on nanoporous BiVO<sub>4</sub> photoelectrode show a significant different trend in Fig. 3a. Interestingly, the optimized BiVO<sub>4</sub>/Ir-COOH photoelectrode exhibited a 2.8 mA/cm<sup>2</sup> photocurrent with ~400 mV lower onset for photocurrent than pristine BiVO<sub>4</sub> (shown in Fig. 3b). Fig. 3a also shows that both the maximum photocurrent and the onset potential of BiVO<sub>4</sub>/Ir-COOH photoelectrode close to the limitation value obtained in BiVO<sub>4</sub>/Na<sub>2</sub>SO<sub>3</sub>.

In contrast, the highly active IrO<sub>x</sub> nanoparticles modified BiVO<sub>4</sub> photoelectrode exhibits worse onset potential and lower photocurrent, which is ~300 mV higher onset potential and much lower photocurrent density than BiVO<sub>4</sub>/Ir-COOH. In fact, the photocurrent density of BiVO<sub>4</sub>/IrO<sub>x</sub> observed is found to be almost the same as its dark current as shown in Fig. S5, and the strange peak of BiVO<sub>4</sub>/IrO<sub>x</sub> observed at 0.8 V vs RHE could be ascribed to the redox peak of IrO<sub>x</sub> nanoparticles. This phenomenon has been commonly found in ligand free hydrolyzed IrO<sub>x</sub> nanoparticle co-catalyzed photoelectrodes. Several reports have suggested that such unexpected result could be explained by iridium hydroxide impurities inducing short-circuit or recombination and could be prevented by covering FTO substrate with a compact under layer [13,17,22].

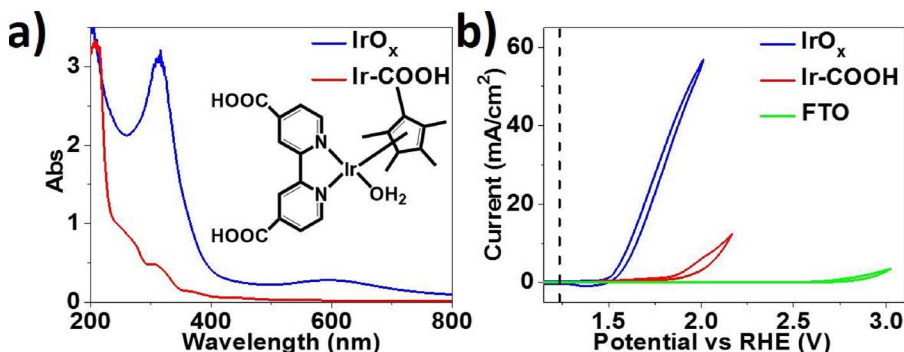


**Fig. 2.** a) UV-vis spectra of 0.1 mM IrO<sub>x</sub> and Ir-COOH in 0.1 M NaOH; b) Cyclic voltammetry curves of Ir-COOH, IrO<sub>x</sub> and FTO in pH 7 phosphate buffered solution (PBS).

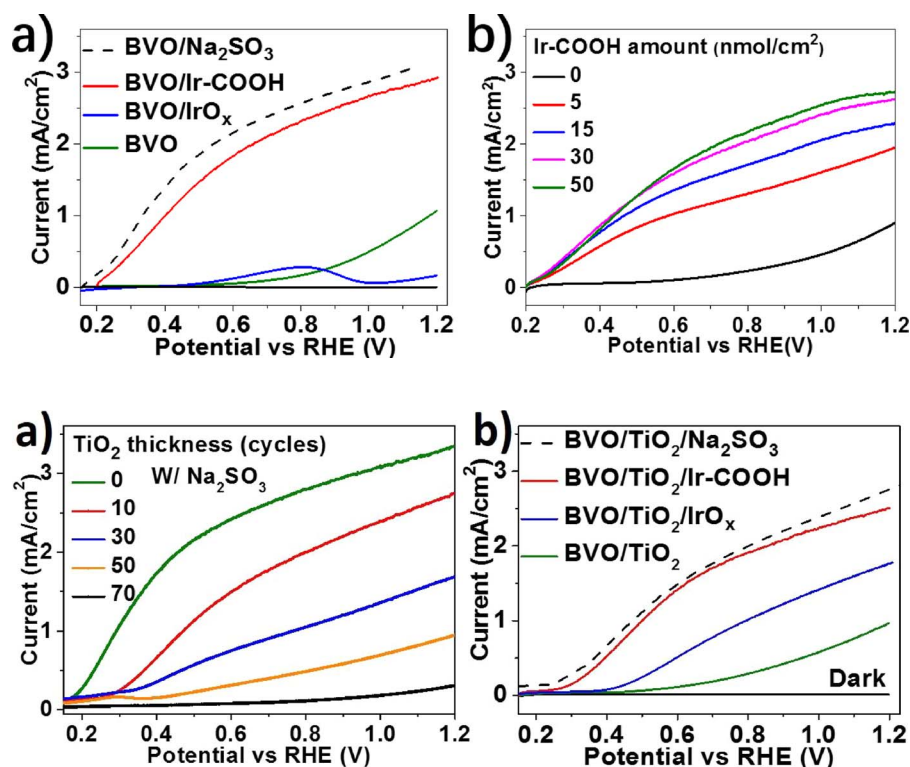


Fig. 3. J-V curves of a) BiVO<sub>4</sub>/Ir-COOH, BiVO<sub>4</sub>/IrO<sub>x</sub> and BiVO<sub>4</sub> in pH 7 PBS under AM 1.5 compared with BiVO<sub>4</sub> in 1 M Na<sub>2</sub>SO<sub>3</sub> compared with bare FTO (dark); b) Optimization of Ir-COOH amount as co-catalysts on BiVO<sub>4</sub>.

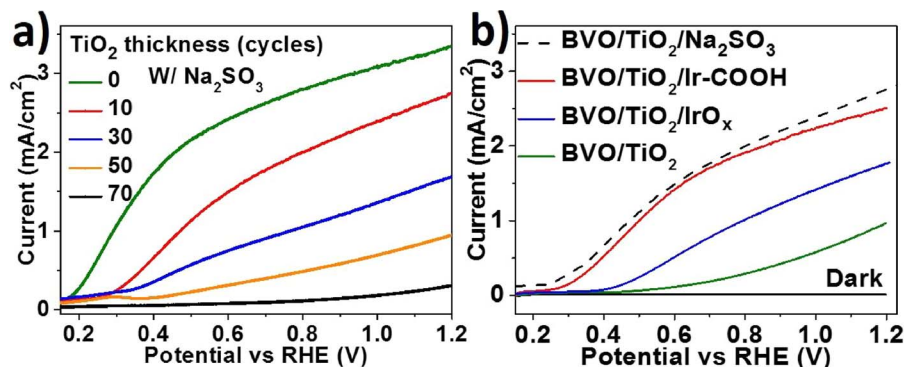


Fig. 4. J-V curves of a) BiVO<sub>4</sub>/TiO<sub>2</sub> for optimization of thickness of TiO<sub>2</sub> in 0.2M pH 7 PBS and b) BiVO<sub>4</sub>/TiO<sub>2</sub>/Ir-COOH, BiVO<sub>4</sub>/TiO<sub>2</sub>/IrO<sub>x</sub> and BiVO<sub>4</sub>/TiO<sub>2</sub> in pH 7 PBS under AM 1.5 compared with J-V curves of BiVO<sub>4</sub> in 1 M Na<sub>2</sub>SO<sub>3</sub>.

### 3.3. Effects of conformal TiO<sub>2</sub> layers on PEC performance

A conformal layer of amorphous TiO<sub>2</sub> was then deposited onto surface of BiVO<sub>4</sub> photoelectrode via atomic layer deposition (ALD) techniques and the optimized deposition cycle number is 10–15 as shown Fig. 4a, which is noted as BiVO<sub>4</sub>/TiO<sub>2</sub>. The deposition of conformal amorphous TiO<sub>2</sub> layer affects both the photocurrent and fill factor of the J-V curve in the case of BiVO<sub>4</sub>/TiO<sub>2</sub>/Na<sub>2</sub>SO<sub>3</sub> and BiVO<sub>4</sub>/TiO<sub>2</sub>/Ir-COOH. However, the conformal TiO<sub>2</sub> layer shows little impact on the PEC performance of BiVO<sub>4</sub> because the dominating factor of low kinetics and high over potential for water oxidation in Fig. S6 [35]. Interestingly, Fig. 4b shows that BiVO<sub>4</sub>/TiO<sub>2</sub>/IrO<sub>x</sub> with optimized IrO<sub>x</sub> have obviously enhanced photocurrent. The optimization of IrO<sub>x</sub> is listed in Fig. S7. However, the best BiVO<sub>4</sub>/TiO<sub>2</sub>/IrO<sub>x</sub> still exhibits more than 100 mV higher onset potential and 30% lower photocurrent than BiVO<sub>4</sub>/TiO<sub>2</sub>/Ir-COOH with the same thick TiO<sub>2</sub> layer.

To explore the difference between the BiVO<sub>4</sub>/TiO<sub>2</sub>/Ir-COOH and BiVO<sub>4</sub>/TiO<sub>2</sub>/IrO<sub>x</sub>, their morphologies were characterized by SEM images as shown in Fig. 5. The top-view SEM image of the BiVO<sub>4</sub>/TiO<sub>2</sub> in Fig. 5a exhibited the same smooth surface as the bare BiVO<sub>4</sub> shown in Fig. 1b. This confirms that the ALD deposited TiO<sub>2</sub> is conformal and uniform, which is similar to previously reported conformal TiO<sub>2</sub> deposited on smooth photoelectrodes. In contrast, Fig. 5b illustrates that the surface of BiVO<sub>4</sub>/TiO<sub>2</sub>/IrO<sub>x</sub> is full of IrO<sub>x</sub> nanoparticles

agglomerates, which is similar to that of BiVO<sub>4</sub>/IrO<sub>x</sub> in Fig. S8. While there is no any morphology difference between BiVO<sub>4</sub>/TiO<sub>2</sub> and BiVO<sub>4</sub>/TiO<sub>2</sub>/Ir-COOH samples in Fig. 5c. This confirmed that Ir-COOH molecules catalysts can be homogeneously distributed and arched onto the surface without agglomerate [25].

The XRD pattern shows no signals for both Ir catalysts and TiO<sub>2</sub> layers as shown in Fig. 6a. However, both EDS mapping results and XPS spectra in Figs. 6b–f and S9 confirm the existence and distribution of elemental Ir and Ti. The TEM images in Fig. 7 further show the BiVO<sub>4</sub> crystal with exposed facets of (200) and (−120) was covered by amorphous TiO<sub>2</sub> layer on other possible facets. Other than the low photocurrent in the J-V curves, the BiVO<sub>4</sub> photoelectrode is always bothered by serious photocurrent decay ascribed to the accumulation of photo-generated holes due to bad transportation and poor water oxidation kinetics, which can be solved by proper doping and using some novel co-catalysts [36,37].

### 3.4. Enhanced performance and stability of BiVO<sub>4</sub>/Ir catalysts with conformal TiO<sub>2</sub> layers

Here, both BiVO<sub>4</sub>/IrO<sub>x</sub> and BiVO<sub>4</sub>/Ir-COOH without the conformal TiO<sub>2</sub> as under layer and interface layer exhibited serious photocurrents decay to near zero in first 100 s as shown in Fig. 8a. With the help of conformal TiO<sub>2</sub> interface layer, BiVO<sub>4</sub>/TiO<sub>2</sub>/IrO<sub>x</sub> and BiVO<sub>4</sub>/TiO<sub>2</sub>/Ir-

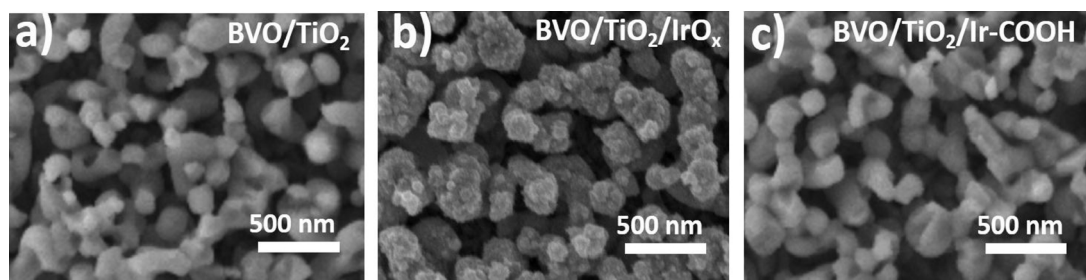


Fig. 5. SEM images of a) BiVO<sub>4</sub>/TiO<sub>2</sub>, b) BiVO<sub>4</sub>/TiO<sub>2</sub>/IrO<sub>x</sub> and c) BiVO<sub>4</sub>/TiO<sub>2</sub>/Ir-COOH.

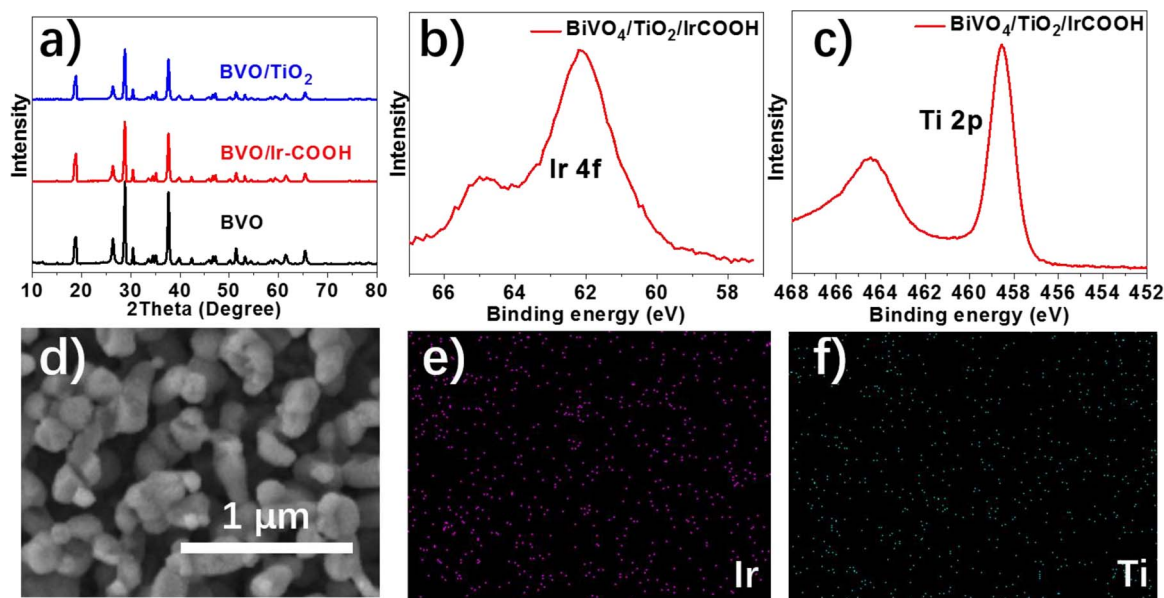


Fig. 6. a) XRD patterns of  $\text{BiVO}_4$  electrodes; b) and c) XPS spectra of  $\text{BiVO}_4/\text{TiO}_2/\text{Ir-COOH}$ ; d) SEM of  $\text{BiVO}_4/\text{TiO}_2/\text{Ir-COOH}/\text{TiO}_2$ ; e) and f) EDS mapping of Ir and Ti.

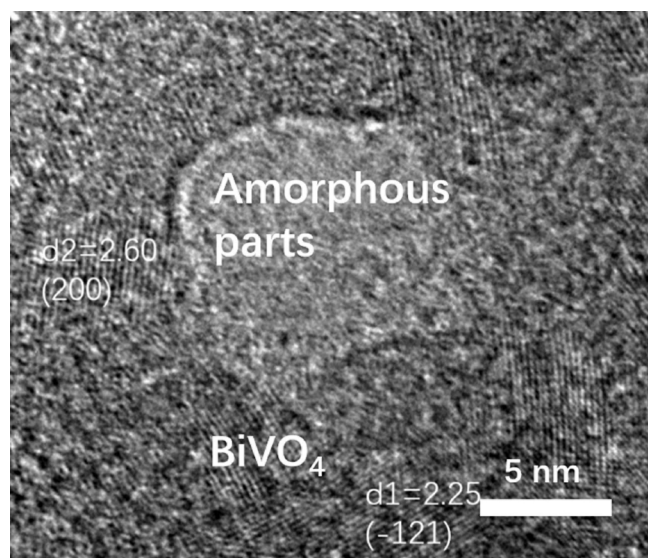


Fig. 7. TEM image of  $\text{BiVO}_4/\text{TiO}_2/\text{Ir-COOH}$ : crystal parts –  $\text{BiVO}_4$  and amorphous parts –  $\text{TiO}_2$ .

COOH showed not only improved initial photocurrents to 1.8 and  $2.7 \text{ mA/cm}^2$  but also the stable currents of 0.4 and  $1.0 \text{ mA/cm}^2$  as shown in Fig. 8b. The photocurrent enhancement can be ascribed to the  $\text{TiO}_2$  passivation effect and improved contact between  $\text{BiVO}_4$  photoelectrode and  $\text{IrO}_x$  or  $\text{Ir-COOH}$  catalysts with the  $\text{TiO}_2$  interlayer.

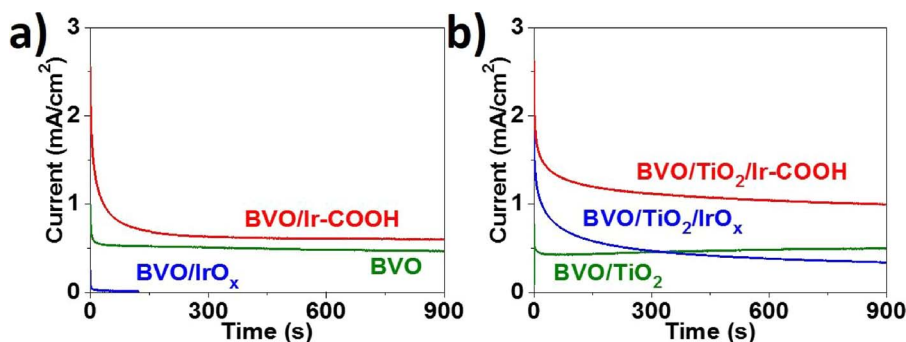


Fig. 8. Constant voltage (I-T curves) of a)  $\text{BiVO}_4$ ,  $\text{BiVO}_4/\text{IrO}_x$  and  $\text{BiVO}_4/\text{Ir-COOH}$ , b)  $\text{BiVO}_4/\text{TiO}_2$ ,  $\text{BiVO}_4/\text{TiO}_2/\text{IrO}_x$  and  $\text{BiVO}_4/\text{TiO}_2/\text{Ir-COOH}$  measured at 1.23 VS RHE in 0.2 M pH 7 PBS under AM 1.5.

However, the interface  $\text{TiO}_2$  layer still did not significantly prevent the decay of photocurrent. The SEM images of  $\text{BiVO}_4/\text{TiO}_2/\text{IrO}_x$  after 10 min photocurrent test in Fig. S7b show serious  $\text{IrO}_x$  nanoparticle peel off. It seems that the peeling off or low stability of  $\text{IrO}_x$  and  $\text{Ir-COOH}$  could be the main reason.

To enhance the stability of these  $\text{IrO}_x$  nanoparticles and  $\text{Ir-COOH}$  molecular catalysts, we deposit another conformal  $\text{TiO}_2$  layer onto  $\text{BiVO}_4/\text{TiO}_2/\text{IrO}_x$  and  $\text{BiVO}_4/\text{TiO}_2/\text{Ir-COOH}$ , which are noted as  $\text{BiVO}_4/\text{TiO}_2/\text{IrO}_x/\text{TiO}_2$  and  $\text{BiVO}_4/\text{TiO}_2/\text{Ir-COOH}/\text{TiO}_2$ . The deposition of the second conformal  $\text{TiO}_2$  layer would hinder electron transfer as confirmed by the J-V curves in Fig. 9a. However, the stable steady photocurrent of  $\text{BiVO}_4/\text{TiO}_2/\text{Ir-COOH}/\text{TiO}_2$  and  $\text{BiVO}_4/\text{TiO}_2/\text{IrO}_x/\text{TiO}_2$  reaches 2.2 and  $1.5 \text{ mA/cm}^2$  (Fig. 9b). This value is significantly higher than  $\text{BiVO}_4/\text{TiO}_2/\text{Ir-COOH}$  and  $\text{BiVO}_4/\text{TiO}_2/\text{IrO}_x$  photoelectrodes, which reveals the protective effect of conformal  $\text{TiO}_2$  layer.

### 3.5. The interface electron transfer property of modified $\text{BiVO}_4/\text{Ir}$ catalysts electrodes

In the above-mentioned double conformal  $\text{TiO}_2$  layers as a protective sandwich configuration, the  $\text{BiVO}_4/\text{TiO}_2/\text{Ir-COOH}/\text{TiO}_2$  shows the highest performance and is even comparable to the  $\text{BiVO}_4/\text{TiO}_2$  tested in  $\text{Na}_2\text{SO}_3$  sacrifice electrolyte. Fig. 10a shows that the electrochemical impedance spectroscopy (EIS) curves of  $\text{BiVO}_4/\text{TiO}_2$  exhibit the highest resistance and the surficial resistance ( $R_{ct}$ ) is up to  $4000 \Omega/\text{cm}^2$ , which can be ascribed to the high over potential for water oxidation without co-catalysts. In contrast,  $\text{BiVO}_4/\text{TiO}_2/\text{Na}_2\text{SO}_3$  systems exhibits the lowest resistance because of negligible over potential for oxidizing

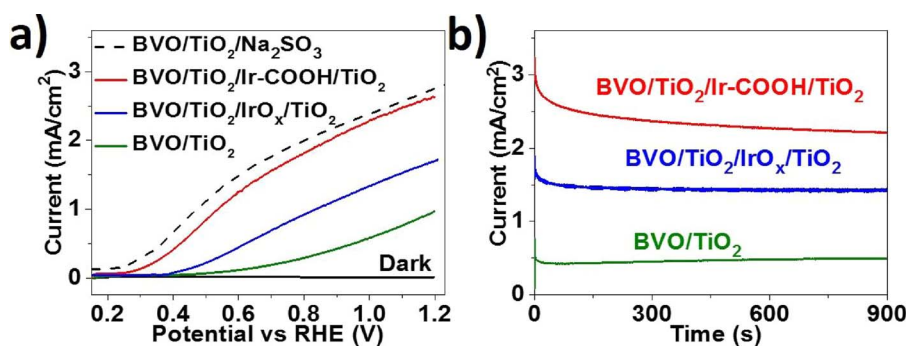


Fig. 9. a) J-V and b) I-T curves of BiVO<sub>4</sub>/TiO<sub>2</sub>, BiVO<sub>4</sub>/TiO<sub>2</sub>/IrO<sub>x</sub>/TiO<sub>2</sub> and BiVO<sub>4</sub>/TiO<sub>2</sub>/Ir-COOH/TiO<sub>2</sub>.

Na<sub>2</sub>SO<sub>3</sub> sacrifice agent. Both BiVO<sub>4</sub>/TiO<sub>2</sub>/IrO<sub>x</sub>/TiO<sub>2</sub> and BiVO<sub>4</sub>/TiO<sub>2</sub>/Ir-COOH/TiO<sub>2</sub> exhibit much lower resistance, which are closed to BiVO<sub>4</sub>/TiO<sub>2</sub>/Na<sub>2</sub>SO<sub>3</sub>. This suggested the importance of co-catalysts to reduce the overpotential for water oxidation reaction. Although the IrO<sub>x</sub> exhibits much better OER catalytic activities than Ir-COOH, the BiVO<sub>4</sub>/TiO<sub>2</sub>/Ir-COOH/TiO<sub>2</sub> shows a lower interface resistance than BiVO<sub>4</sub>/TiO<sub>2</sub>/IrO<sub>x</sub>/TiO<sub>2</sub>. The charge transportation times ( $\tau_d$ ) were characterized by intensity modulated photocurrent spectroscopy (IMPS) as shown in Fig. 10b. Each photoelectrode exhibited a constant charge transportation time independent on photocurrent. Since the photocurrent changes with light intensity linearly, the transportation time shows an independent property to the surficial hole/electrode number reflecting instinct property of electrodes' surfaces. Here, both BiVO<sub>4</sub>/TiO<sub>2</sub>/Ir-COOH/TiO<sub>2</sub> and BiVO<sub>4</sub>/TiO<sub>2</sub>/IrO<sub>x</sub>/TiO<sub>2</sub> photoelectrodes show much faster charge transfer ( $\sim 1$  ms) than BiVO<sub>4</sub>/TiO<sub>2</sub> without any co-catalyst ( $\sim 10$  ms). The charge transfer in BiVO<sub>4</sub>/TiO<sub>2</sub>/Ir-COOH/TiO<sub>2</sub> is  $\sim$  twice faster than the BiVO<sub>4</sub>/TiO<sub>2</sub>/IrO<sub>x</sub>/TiO<sub>2</sub>, which is almost as quick as the BiVO<sub>4</sub>/TiO<sub>2</sub>/Na<sub>2</sub>SO<sub>3</sub>. Here the TiO<sub>2</sub> interface layer has a little impact on the charge transfer change trend. The charge transfer data of BiVO<sub>4</sub> and BiVO<sub>4</sub>/Ir-COOH without double TiO<sub>2</sub> layer are listed in Fig. S10.

Furthermore, the recombination results ( $\tau_n$ ) measured by intensity modulated photovoltage spectroscopy (IMVS) at open circuit were used to reveal the electron lifetime in Fig. 10c. For each half cell, the logarithm of the electron lifetime increases linearly with the photo-induced potential. At the same bias potential at about 0.35 V, the electron

lifetimes increase in the order BiVO<sub>4</sub>/TiO<sub>2</sub>/Ir-COOH/TiO<sub>2</sub> > BiVO<sub>4</sub>/TiO<sub>2</sub>/IrO<sub>x</sub>/TiO<sub>2</sub> > BiVO<sub>4</sub>/TiO<sub>2</sub>. And for each electrode, the charge should not transmit from semiconductors with unexpectedly short charge lifetime ( $\sim 0.02$  s). As a result, BiVO<sub>4</sub>/TiO<sub>2</sub>/IrO<sub>x</sub>/TiO<sub>2</sub> shows almost no photocurrent at 0.35 V vs RHE as shown in Fig. 5a. So the balance between transportation and recombination may account for the different onset potentials [38,39]. The incident photo-to-electron conversion efficiency (IPCE) curves of these different BiVO<sub>4</sub> photoelectrodes are listed in Fig. 10d. The BiVO<sub>4</sub>/TiO<sub>2</sub>/Ir-COOH/TiO<sub>2</sub> reaches  $\sim 50\%$  quantum efficiency, which is close to the up limitation measured for Na<sub>2</sub>SO<sub>3</sub> oxidation. In contrast, the BiVO<sub>4</sub>/TiO<sub>2</sub>/IrO<sub>x</sub>/TiO<sub>2</sub> with worse electron transport properties only exhibited on about half IPCE value as the BiVO<sub>4</sub>/TiO<sub>2</sub>/Ir-COOH/TiO<sub>2</sub>. The IPCE value for BiVO<sub>4</sub>/TiO<sub>2</sub> without co-catalysts is only around 10%, and such low quantum efficiency can be ascribed to the large OER over-potential. All these results indicate that Ir-COOH is more beneficial than IrO<sub>x</sub> on charge transportation in consistence to the higher photocurrents and lower onset potentials.

The above-mentioned electron transfer properties revealed that the interface electron transfer might mainly account for the better performance of the molecular Ir-COOH as co-catalysts for BiVO<sub>4</sub> photoelectrode than IrO<sub>x</sub> nanoparticles. In other word, the interface electron transfer between photoelectrode and co-catalysts might be more important than the co-catalysts' electrochemically catalytic activities. Based on these result, we propose a following schematic mechanism to explain the difference between IrO<sub>x</sub> and Ir-COOH co-catalyzed BiVO<sub>4</sub>

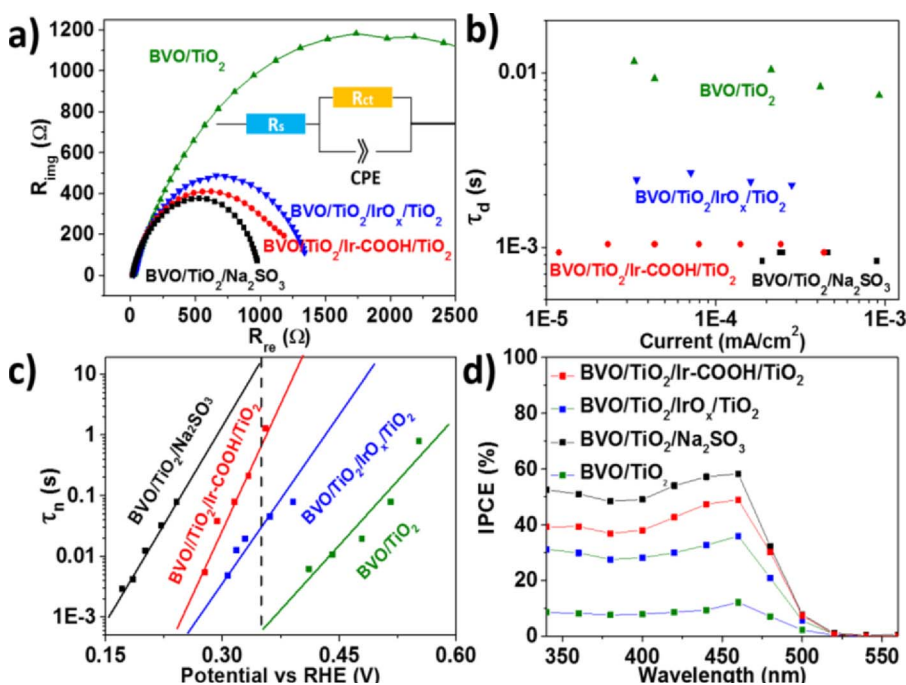


Fig. 10. a) Electrochemical impedance spectrum (EIS) with equivalent circuit diagrams—solution resistance,  $R_{ct}$ —charge transfer resistance and CPE—double layer capacitance, b) IMPS, c) IMVS and d) IPCE data of BiVO<sub>4</sub>/TiO<sub>2</sub>, BiVO<sub>4</sub>/TiO<sub>2</sub>/IrO<sub>x</sub>/TiO<sub>2</sub>, BiVO<sub>4</sub>/TiO<sub>2</sub>/Ir-COOH/TiO<sub>2</sub> and BiVO<sub>4</sub>/TiO<sub>2</sub>/Na<sub>2</sub>SO<sub>3</sub> in followed situation: EIS—0.6 V vs RHE under AM 1.5, IPCE—variable wavelength light source in 0.2 M PBS without Na<sub>2</sub>SO<sub>3</sub>, IMPS—LED 430 nm in 0.2 M PBS.

photoelectrode. Although the size of colloidal  $\text{IrO}_x$  can be as small as 2–5 nm, the deposited  $\text{IrO}_x$  are usually agglomerate on the top surface of the nanoporous  $\text{BiVO}_4$  but the photocharges' diffusion length of undoped  $\text{BiVO}_4$  is short within several hundred nm. The short diffusion length of  $\text{BiVO}_4$  and the inhomogeneous distribution of  $\text{IrO}_x$  nanoparticles then lead to the low co-catalytic performance although these  $\text{IrO}_x$  nanoparticles are the state-of-art OER catalysts with low overpotential. In contrast, the molecular catalysts of Ir-COOH can be homogeneously distributed and anchored onto surface of nanoporous  $\text{BiVO}_4$ . These homogeneously surface distributed Ir-COOH molecular catalysts then could efficiently capture these short diffusion length photo-generated charges in these nanopores. Besides the more efficient charge transfer properties, the molecular catalyst also exhibited atomic utilization efficiency as the dosage of Ir element in  $\text{BiVO}_4/\text{TiO}_2/\text{Ir-COOH}/\text{TiO}_2$  is about 10 times lower than  $\text{BiVO}_4/\text{TiO}_2/\text{IrO}_x/\text{TiO}_2$ . All these results demonstrate the promising advantage of molecular catalysts including better electron transfer and better atomic utility efficiency for PEC application.

#### 4. Conclusions

In summary, we demonstrated that the molecular catalyst of Ir-COOH modified  $\text{BiVO}_4$  electrode showed the excellent photo-electrochemical properties, achieved higher photocurrents and exhibited longer stability with help of sandwiched conformal  $\text{TiO}_2$  layer comparable to the theoretical limitation value using sacrificial agent. The more interesting finding is that the Ir-COOH with lower electrochemically catalytic activities showed significantly catalytic activities especially effective electron transfer properties on the  $\text{BiVO}_4$ . Other than the high efficiency of molecular catalyst of Ir-COOH, the conformal amorphous  $\text{TiO}_2$  layers also enhance the PEC performance of  $\text{BiVO}_4$  photoelectrode by curing the defects, providing anchored sites and protecting the surface to lower the surficial resistance, shorten the transportation time. In all, the combination of sandwiched conformal  $\text{TiO}_2$  layer combined with molecular catalysts would be a promising way to enhance the PEC performance of photoelectrode with higher photo-electron conversion efficiency and better stability.

#### Acknowledgement

YZ acknowledges the support of the NSFC (Grant 21777096).

#### Appendix A. Supplementary data

Supplementary data associated with this article can be found, in the online version, at <https://doi.org/10.1016/j.apcatb.2017.12.014>.

#### References

- [1] M. Grätzel, Photoelectrochemical cells, *Nature* 414 (2001) 338–344.
- [2] J.R. Swierk, T.E. Mallouk, Design and development of photoanodes for water-splitting dye-sensitized photoelectrochemical cells, *Chem. Soc. Rev.* 42 (2013) 2357–2387.
- [3] K. Sivula, R. van de Krol, Semiconducting materials for photoelectrochemical energy conversion, *Nat. Rev. Mater.* (2016) 1–16.
- [4] J. Gu, J.A. Aguiar, S. Ferrere, K.X. Steirer, Y. Yan, C. Xiao, James L. Young, M. Al-Jassim, N.R. Neale, J.A. Turner, A graded catalytic-protective layer for an efficient and stable water-splitting photocathode, *Nat. Energy* 2 (2017) 16192.
- [5] M.G. Walter, E.L. Warren, J.R. McKone, S.W. Boettcher, Q. Mi, E.A. Santori, N.S. Lewis, Solar water splitting cells, *Chem. Rev.* 110 (2010) 6446–6473.
- [6] A.G. Scheuermann, J.P. Lawrence, K.W. Kemp, T. Ito, A. Walsh, C.E.D. Chidsey, P.K. Hurley, P.C. McIntyre, Design principles for maximizing photovoltage in metal-oxide-protected water-splitting photoanodes, *Nat. Mater.* 15 (2016) 99.
- [7] A. Fujishima, Electrochemical photolysis of water at a semiconductor electrode, *Nature* 238 (1972) 37–38.
- [8] S. Oh, J. Oh, High performance and stability of micropatterned oxide-passivated photoanodes with local catalysts for photoelectrochemical water splitting, *J. Phys. Chem. C* 120 (2016) 133–141.
- [9] A. Kudo, K. Ueda, H. Kato, I. Mikami, Photocatalytic  $\text{O}_2$  evolution under visible light irradiation on  $\text{BiVO}_4$  in aqueous  $\text{AgNO}_3$  solution, *Catal. Lett.* 53 (1998) 229–230.
- [10] K. Sayama, A. Nomura, Z. Zou, R. Abe, Y. Abe, H. Arakawa, Photoelectrochemical decomposition of water on nanocrystalline  $\text{BiVO}_4$  film electrodes under visible light, *Chem. Commun.* 290 (2003) 8–290 9.
- [11] T.W. Kim, K.S. Choi, Nanoporous  $\text{BiVO}_4$  photoanodes with dual-layer oxygen evolution catalysts for solar water splitting, *Science* 343 (2014) 990–994.
- [12] F.F. Abdi, L. Han, A.H. Smets, M. Zeman, B. Dam, R. van de Krol, Efficient solar water splitting by enhanced charge separation in a bismuth vanadate-silicon tandem photoelectrode, *Nat. Commun.* 4 (2013) 1–7.
- [13] R. Li, F. Zhang, D. Wang, J. Yang, M. Li, J. Zhu, X. Zhou, H. Han, C. Li, Spatial separation of photogenerated electrons and holes among {010} and {110} crystal facets of  $\text{BiVO}_4$ , *Nat. Commun.* 4 (2013) 1432.
- [14] H. Ye, H.S. Park, A.J. Bard, Screening of electrocatalysts for photoelectrochemical water oxidation on W-doped  $\text{BiVO}_4$  photocatalysts by scanning electrochemical microscopy, *J. Phys. Chem. C* 115 (2011) 12464–12470.
- [15] J.A. Seabold, K. Zhu, N.R. Neale, Efficient solar photoelectrolysis by nanoporous Mo:  $\text{BiVO}_4$  through controlled electron transport, *Phys. Chem. Chem. Phys.* 16 (2014) 1121–1131.
- [16] J. Zhu, F. Fan, R. Chen, H. An, Z. Feng, C. Li, Direct imaging of highly anisotropic photogenerated charge separations on different facets of a single  $\text{BiVO}_4$  photocatalyst, *Angew. Chem. Int. Ed.* 54 (2015) 9111–9114.
- [17] S.P. Berglund, D.W. Flaherty, N.T. Hahn, A.J. Bard, C.B. Mullins, Photoelectrochemical oxidation of water using nanostructured  $\text{BiVO}_4$  films, *J. Phys. Chem. C* 115 (2011) 3794–3802.
- [18] K.J. McDonald, K.S. Choi, A new electrochemical synthesis route for a BiOI electrode and its conversion to a highly efficient porous  $\text{BiVO}_4$  photoanode for solar water oxidation, *Energy Environ. Sci.* 5 (2012) 8553–8557.
- [19] M.N. Shaddad, M.A. Ghanem, A.M. Al-Mayouf, S. Gimenez, J. Bisquert, I. Herranz-Cardona, Cooperative catalytic effect of  $\text{ZrO}_2$  and  $\alpha\text{-Fe}_2\text{O}_3$  nanoparticles on  $\text{BiVO}_4$  photoanodes for enhanced photoelectrochemical water splitting, *Chemosci* 9 (2016) 2779–2783.
- [20] K.-H. Ye, Z. Chai, J. Gu, X. Yu, C. Zhao, Y. Zhang, W. Mai, BiOI- $\text{BiVO}_4$  photoanodes with significantly improved solar water splitting capability: p-n junction to expand solar adsorption range and facilitate charge carrier dynamics, *Nano Energy* 18 (2015) 222–231.
- [21] M. Zhong, T. Hisatomi, Y.B. Kuang, J. Zhao, M. Liu, A. Iwase, Q.X. Jia, H. Nishiyama, T. Minegishi, M. Nakabayashi, N. Shibata, R. Niishiro, C. Katayama, H. Shibano, M. Katayama, A. Kudo, T. Yamada, K. Domen, Surface modification of  $\text{CoO}_x$  loaded  $\text{BiVO}_4$  photoanodes with ultrathin p-type NiO layers for improved solar water oxidation, *J. Am. Chem. Soc.* 137 (2015) 5053–5060.
- [22] Y. Zhao, N.M. Vargas-Barbosa, M.E. Strayer, N.S. McCool, M.-E. Pandelia, T.P. Saunders, J.R. Swierk, J.F. Callejas, L. Jensen, T.E. Mallouk, Understanding the effect of monomeric iridium(III/IV) aquo complexes on the photoelectrochemistry of  $\text{IrO}_x\text{-nH}_2\text{O}$ -catalyzed water-splitting systems, *J. Am. Chem. Soc.* 137 (2015) 8749–8757.
- [23] Y. Kuang, Q. Jia, G. Ma, T. Hisatomi, T. Minegishi, H. Nishiyama, M. Nakabayashi, N. Shibata, T. Yamada, A. Kudo, K. Domen, Ultrastable low-bias water splitting photoanodes via photocorrosion inhibition and in situ catalyst regeneration, *Nat. Energy* 2 (2016) 16191.
- [24] H. Li, Y. Sun, B. Cai, S. Gan, D. Han, L. Niu, T. Wu, Hierarchically Z-scheme photocatalyst of  $\text{Ag@AgCl}$  decorated on  $\text{BiVO}_4$  (040) with enhancing photoelectrochemical and photocatalytic performance, *Appl. Catal. B* 170 (2015) 206–214.
- [25] K.S. Joya, N.K. Subbaiyan, F. D'Souza, H.J. de Groot, Surface-immobilized single-site iridium complexes for electrocatalytic water splitting, *Angew. Chem. Int. Ed.* 51 (2012) 9601–9605.
- [26] M.D. Karkas, O. Verho, E.V. Johnston, B. Akermark, Artificial photosynthesis molecular systems for catalytic water oxidation, *Chem. Rev.* 114 (2014) 11863–12001.
- [27] O. Diaz-Morales, T.J.P. Hersbach, D.G.H. Hetterscheid, J.N.H. Reek, M.T.M. Koper, Electrochemical and spectroelectrochemical characterization of an iridium-based molecular catalyst for water splitting: turnover frequencies, stability, and electrolyte effects, *J. Am. Chem. Soc.* 136 (2014) 10432–10439.
- [28] J.D. Blakemore, R.H. Crabtree, G.W. Brudvig, Molecular catalysts for water oxidation, *Chem. Rev.* 115 (2015) 12974–13005.
- [29] J. Gu, Y. Yan, J.L. Young, K.X. Steirer, N.R. Neale, J.A. Turner, Water reduction by a p-GaInP<sub>2</sub> photoelectrode stabilized by an amorphous  $\text{TiO}_2$  coating and a molecular cobalt catalyst, *Nat. Mater.* (2015) 1–7.
- [30] M.T. McDowell, M.F. Lichterman, J.M. Spurgeon, S. Hu, I.D. Sharp, B.S. Brunschwig, N.S. Lewis, Improved stability of polycrystalline bismuth vanadate photoanodes by use of dual-layer thin  $\text{TiO}_2/\text{Ni}$  coatings, *J. Phys. Chem. C* 118 (2014) 19618–19624.
- [31] D. Eisenberg, H.S. Ahn, A.J. Bard, Enhanced photoelectrochemical water oxidation on bismuth vanadate by electrodeposition of amorphous titanium dioxide, *J. Am. Chem. Soc.* 136 (2014) 14011–14014.
- [32] H. Li, H. Yu, X. Quan, S. Chen, H. Zhao, Improved photocatalytic performance of heterojunction by controlling the contact facet: high electron transfer capacity between  $\text{TiO}_2$  and the {110} facet of  $\text{BiVO}_4$  caused by suitable energy band alignment, *Adv. Funct. Mater.* 25 (2015) 3074–3080.
- [33] A.P. Singh, N. Kodan, B.R. Mehta, A. Held, L. Mayrhofer, M. Moseler, Band edge engineering in  $\text{BiVO}_4/\text{TiO}_2$  heterostructure: enhanced photoelectrochemical performance through improved charge transfer, *ACS Catal.* 6 (2016) 5311–5318.
- [34] V. Nair, C.L. Perkins, Q. Lin, M. Law, Textured nanoporous Mo:  $\text{BiVO}_4$  photoanodes with high charge transport and charge transfer quantum efficiencies for oxygen evolution, *Energy Environ. Sci.* 9 (2016) 1412–1429.
- [35] X. Zhu, F. Zhang, M. Wang, X. Gao, Y. Luo, J. Xue, Y. Zhang, J. Ding, S. Sun, J. Bao, C. Gao, A shuriken-shaped m- $\text{BiVO}_4$ /{001}- $\text{TiO}_2$  heterojunction: synthesis, structure and enhanced visible light photocatalytic activity, *Appl. Catal. A* 521 (2016) 42–49.

- [36] J.A. Seabold, K.S. Choi, Efficient and stable photo-oxidation of water by a bismuth vanadate photoanode coupled with an iron oxyhydroxide oxygen evolution catalyst, *J. Am. Chem. Soc.* 134 (2012) 2186–2192.
- [37] J. Su, Z. Bai, B. Huang, X. Quan, G. Chen, Unique three dimensional architecture using a metal-free semiconductor cross-linked bismuth vanadate for efficient photoelectrochemical water oxidation, *Nano Energy* 24 (2016) 148–157.
- [38] J. Wang, I. Mora-Sero, Z. Pan, K. Zhao, H. Zhang, Y. Feng, G. Yang, X. Zhong, J. Bisquert, Core/shell colloidal quantum dot exciplex states for the development of highly efficient quantum-dot-sensitized solar cells, *J. Am. Chem. Soc.* 135 (2013) 15913–15922.
- [39] T. Li, J. He, B. Pena, C.P. Berlinguette, Curing BiVO<sub>4</sub> photoanodes with ultraviolet light enhances photoelectrocatalysis, *Angew. Chem. Int. Ed.* 55 (2016) 1769–1772.